

Superconducting phase diagram of Sb and Se substitution in CeOBiS<sub>2</sub> single crystals

Tatsuya Suzuki<sup>1</sup>, Masanori Nagao<sup>1\*</sup>, Yuki Maruyama<sup>1</sup>, Satoshi Watauchi<sup>1</sup>, and Isao Tanaka<sup>1</sup>

<sup>1</sup>*University of Yamanashi, 7-32 Miyamae, Kofu, Yamanashi 400-0021, Japan*

\*Corresponding Author

Masanori Nagao

Postal address: University of Yamanashi, Center for Crystal Science and Technology

Miyamae 7-32, Kofu, Yamanashi 400-0021, Japan

Telephone number: (+81)55-220-8610

Fax number: (+81)55-220-8270

E-mail address: mnagao@yamanashi.ac.jp

## **Abstract**

Sb- and Se-substituted CeOBiS<sub>2</sub> single crystals have been successfully grown using CsCl/KCl flux. Sb and Se substitution dependence of the superconductivity on CeOBiS<sub>2</sub> was investigated and the superconducting phase diagram at above 0.3 K was described. The non-linear boundary between superconductivity and non-superconductivity was revealed.

## Main text

### 1. Introduction

Layered superconductors exhibited high transition temperatures such as cuprate<sup>1)</sup> and iron-based superconductors.<sup>2)</sup> CeOBiS<sub>2</sub> is one of the BiS<sub>2</sub>-based layered superconductors such as La(O,F)BiS<sub>2</sub><sup>3)</sup> which is a layered superconductor. Several BiS<sub>2</sub>-based layered compounds with superconductivity require the F substitution in the O-site for the electron carrier introduction. Among them, CeOBiS<sub>2</sub> without F substitution exhibits superconductivity by the Ce valence fluctuation.<sup>4,5)</sup> The Ce valence fluctuation formed at of Ce<sup>3+</sup> and Ce<sup>4+</sup> mixing valence state was observed by X-ray photoelectron spectroscopy (XPS)<sup>5)</sup> and X-ray absorption spectroscopy (XAS).<sup>6)</sup> Furthermore, the temperature dependence of resistivity at a normal state was reported weak semiconducting-like behavior.<sup>4,5)</sup> On the other hand, the CeOBiS<sub>2</sub> with Arrhenius-type behavior at a normal state resistivity was reported no superconductivity.<sup>7)</sup> This difference was explained by the existence of two kinds of local structure configurations in the CeOBiS<sub>2</sub> which intrinsically exhibited semiconducting behavior, but a metallic phase appeared due to the local distortions.<sup>8)</sup> Therefore, we focused on the superconducting CeOBiS<sub>2</sub> which was a simple chemical formulation in BiS<sub>2</sub>-based layered superconductors. Previously we found the superconductivity was

suppressed with Sb substitution into the Bi-site, which is presumed to originate from the change of the crystal system.<sup>9)</sup> In contrast, the CeOBiS<sub>2</sub> superconductor with Se substitution into the S-site exhibited enhancement of in-plane chemical pressure<sup>10)</sup>, suppression of in-plane disorder, and decrease of Ce ions valence. As a result, an increase in superconducting transition temperature was observed.<sup>11)</sup> Especially, the in-plane chemical pressure increases the density of states at the Fermi level, which may increase the phonon frequency. The possibility of the enhancement of superconductivity by these phenomena was suggested.<sup>10)</sup>

In this paper, the effect of both Sb and Se substitutions for superconductivity at above 0.3 K was systematically investigated using the Sb- and Se-substituted CeOBiS<sub>2</sub> [CeO(Bi,Sb)(S,Se)<sub>2</sub>] single crystals. Then superconducting phase diagram of Sb and Se substitution in CeOBiS<sub>2</sub> was revealed.

## 2. Experimental Details

Sb- and Se-substituted CeOBiS<sub>2</sub> [CeO(Bi,Sb)(S,Se)<sub>2</sub>] single crystals were grown using CsCl/KCl flux.<sup>4,12,13)</sup> The raw materials of Ce<sub>2</sub>S<sub>3</sub>, Bi<sub>2</sub>O<sub>3</sub>, Bi<sub>2</sub>S<sub>3</sub>, Bi, Sb (or Sb<sub>2</sub>O<sub>3</sub>), and Se were weighed to a total amount of 0.8 g for a nominal composition of CeOBi<sub>1-x</sub>Sb<sub>x</sub>S<sub>2-y</sub>Se<sub>y</sub> ( $0 \leq x \leq 0.20$ ,  $0.125 \leq y \leq 0.500$ ). The molar ratio of the CsCl/KCl

flux was CsCl:KCl = 5:3 with a total amount of 5.0 g. The raw materials (0.8 g) and CsCl/KCl flux (5.0 g) were mixed and ground using a mortar and then sealed in an evacuated quartz tube (~10 Pa). The prepared quartz tube was heated at 950 °C (Except for  $x = 0$ ,  $y = 0.500$ , which was performed at 1000 °C.) for 10 h, followed by cooling to 600 °C at a rate of 1 °C/h, then the sample was spontaneously cooled down to room temperature (~30 °C) in the furnace. The heated quartz tube was opened to air and the obtained materials were washed and filtered to remove the CsCl/KCl flux using distilled water.

The obtained crystals confirmed the CeOBiS<sub>2</sub> structure<sup>5)</sup> by X-ray diffraction (XRD) (Rigaku; MultiFlex) with CuK $\alpha$  radiation. The compositional ratio of the grown crystals was evaluated using energy dispersive X-ray spectrometry (EDS) (Bruker; Quantax 70) associated with the observation of the microstructure, based on scanning electron microscopy (SEM) (Hitachi High-Technologies; TM3030). Analytical compositions of each element were defined as  $C_{XX}$  ( $XX$ : Bi, Sb, S, and Se). The obtained compositional values were normalized using  $C_S + C_{Se} = 2$  (S + Se analytical composition was 2), and then Bi, and Sb compositions ( $C_{Bi}$ , and  $C_{Sb}$ ) were determined.

The picked single crystals at random from each sample lot were measured the resistivity–temperature ( $\rho$ – $T$ ) characteristics. The  $\rho$ – $T$  characteristics of the picked

single crystals were determined using the standard four-probe method with a constant current density mode range of 20–50 mA/cm<sup>2</sup> using a physical property measurement system (Quantum Design; PPMS DynaCool). The electrical terminals were fabricated using Ag paste (DuPont; 4922N). The  $\rho$ - $T$  characteristics in the temperature range of 0.3–15 K were evaluated based using the adiabatic demagnetization refrigerator (ADR) option for the PPMS. A magnetic field of 3.0 T at 1.9 K was applied to operate the ADR, which was subsequently removed. Consequently, the temperature of the sample decreased to approximately 0.3 K. The measurement of  $\rho$ - $T$  characteristics was initiated at the lowest temperature (~0.3 K), which was spontaneously increased to 15 K. The superconducting transition temperature with zero resistivity ( $T_c^{zero}$ ) was estimated from the  $\rho$ - $T$  characteristics. The  $T_c^{zero}$  was determined as the temperature at which the resistivity is below approximately 300  $\mu\Omega\text{cm}$  (Except for  $C_{\text{Sb}} = 0.068$ ,  $C_{\text{Se}} = 0.28$ , which was determined at 3.0 m $\Omega\text{cm}$  due to a technical problem.). The compositional ratio of the  $\rho$ - $T$  characteristics measured samples had been evaluated by EDS, and then they were employed for the superconducting phase diagram.

### 3. Results and Discussion

The obtained CeO(Bi,Sb)(S,Se)<sub>2</sub> single crystals exhibited a plate-like shape with a

size of approximately 1.0 mm and a thickness of 100–200  $\mu\text{m}$ , which were similar in shape to Sb-substituted  $\text{CeOBiS}_2$  [ $\text{CeO}(\text{Bi},\text{Sb})\text{S}_2$ ] single crystals.<sup>9)</sup> However, the well-developed plane in  $\text{CeO}(\text{Bi},\text{Sb})(\text{S},\text{Se})_2$  single crystals was rougher than that of  $\text{CeO}(\text{Bi},\text{Sb})\text{S}_2$  single crystals. A well-developed plane in the obtained  $\text{CeO}(\text{Bi},\text{Sb})(\text{S},\text{Se})_2$  single crystals corresponded to the *c*-plane of  $\text{CeOBiS}_2$  structure<sup>4)</sup> by the XRD patterns. The *c*-axis lattice parameters for the obtained  $\text{CeO}(\text{Bi},\text{Sb})(\text{S},\text{Se})_2$  single crystals were range of 13.53–13.62 Å with depending on both Sb and Se substitution amount. Analytical compositions of Sb and Se in the obtained  $\text{CeO}(\text{Bi},\text{Sb})(\text{S},\text{Se})_2$  single crystals were lower than those of the nominal compositions, and these analytical compositions exhibited dispersion in the same grown lot. Table I summarized the nominal (*x* and *y*) and analytical ( $C_{\text{Bi}}$ ,  $C_{\text{Sb}}$ ,  $C_{\text{S}}$ , and  $C_{\text{Se}}$ ) compositions with normalized using  $C_{\text{S}} + C_{\text{Se}} = 2$  for the  $\text{CeO}(\text{Bi},\text{Sb})(\text{S},\text{Se})_2$  single crystals. All samples exhibited the Bi-site deficiency which was observed  $C_{\text{Bi}} + C_{\text{Sb}} < 1$ . The amount of Bi-site deficiency was in the range of 4–9 at% which was a similar range of the only Sb-substituted  $\text{CeOBiS}_2$  [ $\text{CeO}(\text{Bi},\text{Sb})\text{S}_2$ ] single crystals.<sup>9)</sup> The Bi-site deficiency values were higher than  $\text{CeOBiS}_2$  without Sb substitution,<sup>14,15)</sup> this indicated that Sb substitution enhanced the Bi-site deficiency in the  $\text{CeOBiS}_2$  structure. Besides, we investigated the compositions of the obtained  $\text{CeO}(\text{Bi},\text{Sb})(\text{S},\text{Se})_2$  single crystals into the

difference of Sb source which was Sb or  $\text{Sb}_2\text{O}_3$ . And then this result hardly changed.

The  $\text{CeO}(\text{Bi},\text{Sb})(\text{S},\text{Se})_2$  single crystals at random in each lot grown from each nominal composition were picked, and the  $\rho-T$  measurements and compositional analysis were performed for the superconducting phase diagram investigation. The  $\rho-T$  characteristics of some typical  $\text{CeO}(\text{Bi},\text{Sb})(\text{S},\text{Se})_2$  single crystals were shown in Figure 1. Weak semiconducting-like behavior at near above superconducting transition temperature in a normal state was observed. At first glance, a correlation between normal state resistivity and superconducting transition temperature seems to exist. However, in the case of the samples without superconducting transition (Ex.  $C_{\text{Sb}} = 0.05$ ,  $C_{\text{Se}} = 0.09$ ), the normal state resistivity was lower than that of superconducting samples. Then the relationship between normal state resistivity and superconductivity was unclear in this experiment. Figure 2 shows the superconducting phase diagram of Sb and Se substitution dependence for  $\text{CeO}(\text{Bi},\text{Sb})(\text{S},\text{Se})_2$  single crystals. The data of  $\text{CeO}(\text{Bi},\text{Sb})\text{S}_2$  single crystals were referred from Ref. 9. The superconducting transition temperature with zero resistivity ( $T_{\text{c}}^{\text{zero}}$ ) was decreased with the increase in Sb substitution and increased with the increase in Se substitution. Superconductivity in  $\text{CeOBiS}_2$  was suppressed as the Sb substitution, enhanced by the Se substitution. Those behaviors exhibited the same trend as previous reports.<sup>9,11)</sup> In other words, the Sb

substitution region with superconducting observation was spread by the Se substitution. The boundary between superconductivity and non-superconductivity at above 0.3 K showed non-linear which is plotted in the dashed line in Figure 2 (b). That boundary showed the dome shape at  $C_{\text{Se}} = 0.15\text{--}0.30$  region which increased the  $T_c^{\text{zero}}$ . Se-substituted CeOBiS<sub>2</sub> [CeOBi(S,Se)<sub>2</sub>] superconducting phase diagram showed a similar dome shape which originated from the in-plane chemical pressure effects<sup>10)</sup> and decrease of carrier concentration due to the Ce valence state.<sup>11)</sup> We assumed that the dome shape behavior of superconducting transition temperature in Figure 2 (b) originated from the same phenomena.

#### 4. Conclusion

Sb- and Se-substituted CeOBiS<sub>2</sub> [CeO(Bi,Sb)(S,Se)<sub>2</sub>] single crystals were grown and measured the superconducting transition temperature. A superconducting phase diagram with  $C_{\text{Sb}} < 0.18$ ,  $C_{\text{Se}} < 0.45$  for CeOBiS<sub>2</sub> was revealed. The boundary between superconductivity and non-superconductivity at above 0.3 K showed a non-linear line with the dome shape at  $C_{\text{Se}} = 0.15\text{--}0.30$  region.

#### Acknowledgments

This work was supported by JSPS KAKENHI (Grant-in-Aid for Scientific Research (B) and (C): Grant Number 21H02022, 19K05248, and 23K03358, Grant-in-Aid for Challenging Exploratory Research: Grant Number 21K18834).

## References

- 1) J. B. Bednorz and K. Müller, *Z. Phys. B* **64**, 189–193 (1986).
- 2) Y. Kamihara, T. Watanabe, M. Hirano, and H. Hosono, *J. Am. Chem. Soc.* **130**, 3296–3297 (2008).
- 3) Y. Mizuguchi, S. Demura, K. Deguchi, Y. Takano, H. Fujihisa, Y. Gotoh, H. Izawa, and O. Miura, *J. Phys. Soc. Jpn.* **81**, 114725 (2012).
- 4) M. Nagao, A. Miura, I. Ueta, S. Watauchi, and I. Tanaka, *Solid State Commun.* **245**, 11–14 (2016).
- 5) M. Tanaka, M. Nagao, R. Matsumoto, N. Kataoka, I. Ueta, H. Tanaka, S. Watauchi, I. Tanaka, and Y. Takano, *J. Alloys Compd.* **722**, 467–473 (2017).
- 6) T. Sugimoto, B. Joseph, E. Paris, A. Iadecola, T. Mizokawa, S. Demura, Y. Mizuguchi, Y. Takano, and N. L. Saini, *Phys. Rev. B* **89**, 201117(R) (2014).
- 7) R. Higashinaka, T. Asano, T. Nakashima, K. Fushiya, Y. Mizuguchi, O. Miura, T. D. Matsuda, and Y. Aoki, *J. Phys. Soc. Jpn.* **84**, 023702 (2015).
- 8) T. Sugimoto, E. Paris, T. Wakita, K. Terashima, T. Yokoya, A. Barinov, J. Kajitani, R. Higashinaka, T. D. Matsuda, Y. Aoki, T. Mizokawa, and N. L. Saini, *Sci Rep* **8**, 2011 (2018).
- 9) T. Suzuki, Y. Hanada, M. Nagao, Y. Maruyama, S. Watauchi, and I. Tanaka, *Solid*

State Commun. **378**, 115414 (2024).

- 10) Y. Mizuguchi, A. Miura, J. Kajitani, T. Hiroi, O. Miura, K. Tadanaga, N. Kumada, E. Magome, C. Moriyoshi, and Y. Kuroiwa, Sci. Rep. **5**, 14968 (2015).
- 11) R. Kiyama, Y. Goto, K. Hoshi, R. Jha, A. Miura, C. Moriyoshi, Y. Kuroiwa, T. D. Matsuda, Y. Aoki, and Y. Mizuguchi, J. Phys. Soc. Jpn. **89**, 064702 (2020).
- 12) M. Nagao, S. Demura, K. Deguchi, A. Miura, S. Watauchi, T. Takei, Y. Takano, N. Kumada, and I. Tanaka, J. Phys. Soc. Jpn. **82**, 113701 (2013).
- 13) M. Nagao, M. Tanaka, R. Matsumoto, H. Tanaka, S. Watauchi, Y. Takan, and I. Tanaka, Cryst. Growth Des. **16**, 3037–3042 (2016).
- 14) A. Miura, M. Nagao, T. Takei, S. Watauchi, I. Tanaka, and N. Kumada, J. Solid Chem. **212**, 213–217 (2014).
- 15) T. Machida, Y. Fujisawa, M. Nagao, S. Demura, K. Deguchi, Y. Mizuguchi, Y. Takano, and H. Sakata, J. Phys. Soc. Jpn. **83**, 113701 (2014).

### **Figure caption**

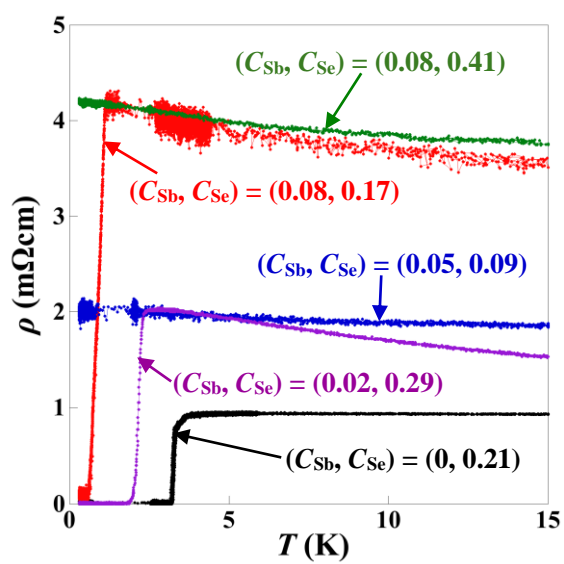
Figure 1 (Color online) Resistivity–temperature ( $\rho-T$ ) characteristics of typical  $\text{CeO}(\text{Bi},\text{Sb})(\text{S},\text{Se})_2$  single crystals.

Figure 2 (Color online) (a) Superconducting phase diagram of Sb- and Se-substituted composition ( $C_{\text{Sb}}$  and  $C_{\text{Se}}$ ) for  $\text{CeOBiS}_2$  single crystals (b) projection of  $C_{\text{Sb}}-C_{\text{Se}}$  plane. The data of  $\text{CeO}(\text{Bi},\text{Sb})\text{S}_2$  single crystals were referred from Ref. 9.

Table I Nominal Sb and Se composition ( $x$  and  $y$ ), and analytical composition ( $C_{\text{Bi}}$ ,  $C_{\text{Sb}}$ ,  $C_{\text{S}}$ , and  $C_{\text{Se}}$ ) in the obtained crystals. ( $C_{\text{Bi}}$ ,  $C_{\text{Sb}}$ ,  $C_{\text{S}}$ , and  $C_{\text{Se}}$  compositions were normalized by  $C_{\text{S}} + C_{\text{Se}} = 2$ .)

Nominal composition		Analytical composition (Normalized using $C_{\text{Sb}} + C_{\text{Se}} = 2$ )			
Sb: $x$	Se: $y$	$C_{\text{Bi}}$	$C_{\text{Sb}}$	$C_{\text{S}}$	$C_{\text{Se}}$
0	0.125	0.95±0.02	0.00±0.00	1.89±0.02	0.11±0.02
0.050	0.125	0.92±0.02	0.02±0.01	1.91±0.02	0.09±0.02
0.050*	0.125	0.93±0.04	0.03±0.02	1.92±0.03	0.08±0.03
0.075	0.125	0.89±0.04	0.05±0.01	1.91±0.02	0.09±0.02
0.100	0.125	0.85±0.01	0.08±0.03	1.87±0.01	0.13±0.01
0.100*	0.125	0.87±0.02	0.05±0.02	1.91±0.02	0.09±0.02
0.150*	0.125	0.82±0.02	0.11±0.02	1.90±0.01	0.10±0.01
0	0.250	0.96±0.02	0.00±0.00	1.79±0.02	0.21±0.02
0.050	0.250	0.90±0.03	0.02±0.01	1.80±0.02	0.20±0.02
0.075	0.250	0.88±0.04	0.05±0.01	1.81±0.01	0.19±0.01
0.100	0.250	0.87±0.04	0.09±0.05	1.84±0.02	0.16±0.02
0.150	0.250	0.84±0.06	0.11±0.05	1.83±0.06	0.17±0.06
0	0.375	0.95±0.01	0.00±0.00	1.70±0.01	0.31±0.01
0.050	0.375	0.93±0.02	0.02±0.01	1.72±0.02	0.29±0.02
0.075	0.375	0.86±0.04	0.06±0.04	1.63±0.05	0.37±0.05
0.100	0.375	0.89±0.02	0.04±0.01	1.70±0.02	0.29±0.02
0.125	0.375	0.82±0.09	0.09±0.05	1.72±0.04	0.28±0.04
0.150	0.375	0.83±0.05	0.11±0.06	1.66±0.02	0.34±0.02
0	0.500	0.94±0.01	0.00±0.00	1.59±0.03	0.41±0.03
0.050	0.500	0.90±0.02	0.04±0.02	1.63±0.02	0.37±0.02
0.100	0.500	0.88±0.04	0.06±0.01	1.60±0.02	0.40±0.02
0.125	0.500	0.86±0.02	0.08±0.01	1.59±0.03	0.41±0.03
0.150	0.500	0.84±0.06	0.11±0.03	1.60±0.03	0.40±0.03
0.200	0.500	0.77±0.04	0.15±0.02	1.57±0.03	0.43±0.03

\*: Sb source was employed as  $\text{Sb}_2\text{O}_3$ .



**Figure 1**

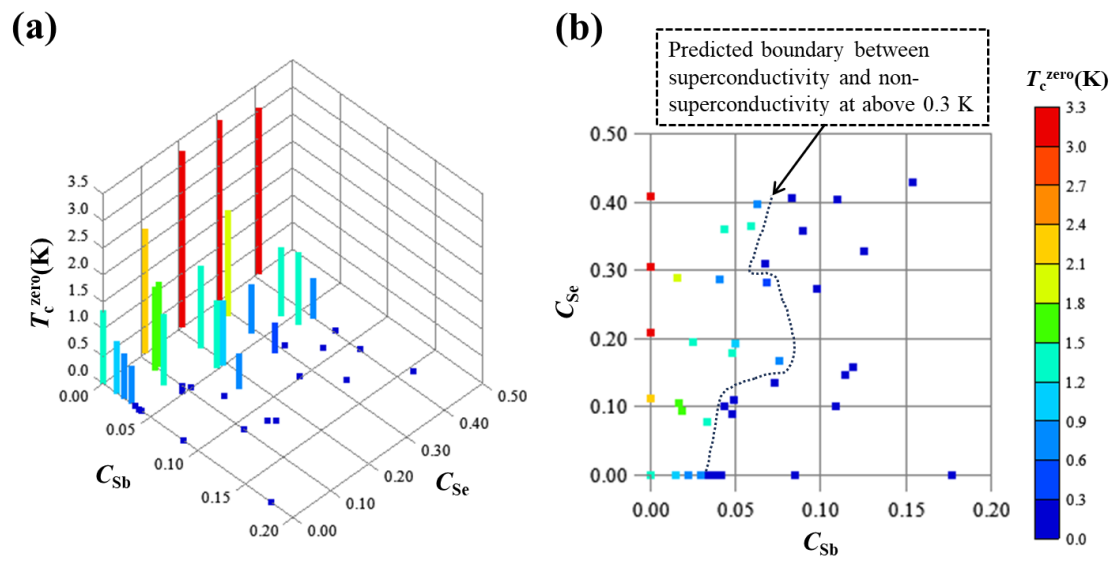


**Figure 2**